Tribological and mechanical properties of high power laser surface-treated metallic glasses

Matthews, D. T. A.; Ocelik, V.; de Hosson, J. Th. M.

Published in:
Materials science and engineering a-Structural materials properties microstructure and processing

DOI:
10.1016/j.msea.2007.02.119

Publication date:
2007

ELSEVIER

Materials Science and Engineering A 471 (2007) 155–164

MATERIALS SCIENCE & ENGINEERING A

www.elsevier.com/locate/msea

Tribological and mechanical properties of high power laser surface-treated metallic glasses

D.T.A. Matthews, V. Ocelík, J.Th.M. de Hosson *

Department of Applied Physics and Netherlands Institute for Metals Research, University of Groningen, Nijenborgh 4, Groningen 9474 AG, The Netherlands

Received 12 March 2006; received in revised form 16 February 2007; accepted 21 February 2007

Abstract

The processing power of high power Nd:YAG laser has been utilised to achieve the inherently high cooling rates required to form many of today's bulk metallic glasses (BMGs). The production of thick (≥250 μm) amorphous surface layers has been considered. Microstructural and chemical observation techniques including scanning electron microscopy (SEM) and transmission electron microscopy (both with energy-dispersive X-ray spectrometry, EDS), and X-ray diffraction (XRD), reveal that fully amorphous layers are attainable. Coating-to-substrate adherence is functionally graded by virtue of an amorphous matrix interlayer around 50 μm in depth. Actual cladding and remelting to Ti substrates indicate that the process of laser cladding is a suitable technique for the application of metallic glasses as surface layers. Hardness and nanoindentation profiles reveal hardnesses up to 13 GPa over the full depth of a coating, coupled with elastic modulus around 150 GPa, which are comparable with bulk metallic glass melt–spun ribbons. Tribological tests have also been conducted which reveal good wear properties are attainable and shear banding has been seen in the contact region. Scratch testing shows the layers may exhibit extremely low coefficients of friction, and again shear band formation is witnessed.

Keywords: Laser surface treatment; Metallic glass; Sliding wear; Hardness

1. Introduction

Bulk metallic glasses (BMGs) have been the subjects of widespread investigations in recent times, due to their improved properties over crystalline materials, induced through the absence of grain boundaries. These improvements include high compressive strength, high hardness and excellent corrosion resistance, amongst others. Extensive work has been conducted on glass-forming systems such as the Cu–Ti–Zr–Ni based system first purported by Lin and Johnson [1]. One variation on this system is the glass-forming alloy (GFA) $Cu_{47}Ti_{33}Zr_{11}Ni_6Sn_2Si_1$ (numbers indicate at.%). Park et al. [2] found that the partial substitution of Ni with Sn addition in the form $Cu_{47}Ti_{33}Zr_{11}Ni_{8-x}Sn_xSi_1$ improved the glass-forming ability of the system, with an increasing critical casting diameter from 4 to 6 mm when processing by injection casting for the composition $Cu_{47}Ti_{33}Zr_{11}Ni_6Sn_2Si_1$. This improved critical casting result implies that the critical cooling rate required to achieve amorphicity is reduced. This is one of the most important parameters when considering metallic glass formation since reduced cooling rates facilitate a wider range of processing options.

An entire work-piece should rarely need to be formed wholly from one material, since most manufactured articles are only functional at their surface. By harnessing the properties of selected BMGs in the surfaces of tribologically poor materials (such as titanium and aluminium) these materials can be exploited in many more diverse ranges of applications than they currently find. High power lasers have become increasingly accepted as tools for many applications from cutting, to welding to surface modification methods [3]. The high power laser has been proven to be capable of producing adherent, hard, wear corrosion fatigue and fracture resistant coatings on a diverse range of materials [4–6].

The cooling rates also afforded by high power lasers [7,8] in local areas are certainly in the bounds of the quench rates necessary for "amorphisation", and hence surface engineering by high power laser provides the chosen tool for this investigation

* Corresponding author. Tel.: +31 50 3634898; fax: +31 50 3634881.
E-mail address: j.t.m.de.hosson@rug.nl (J.Th.M. de Hosson).

0921-5093/$ – see front matter © 2007 Elsevier B.V. All rights reserved.
doi:10.1016/j.msea.2007.02.119

into the fabrication of functionally graded amorphous surface layers. The associated adhesion properties of a functionally graded material (FGM) ensure the prospects are also exciting [9]. Numerous BMG compositions have been published to date, however, the subject of our intrigue, as stated previously, has been not only the possibility of producing metallic glasses, but producing glassy metallic surface layers by high power laser. Our main impetus is behind Ti-rich or Ti-containing compositions, driven with the motivation that we may utilise laser cladding to improve the inherently poor tribological properties of titanium. Aluminium is also an interesting substrate material, as is iron. Many of the BMG compositions published contain Zr, which is often used in tandem with Be, as this element considerably improves the glass-forming ability of Zr-containing alloys [10,11] by strong bonding between Zr–Be atomic pairs which suppress the formation of competing crystalline phases during solidification. Beryllium, however, unfortunately forms harmful (cancerous) oxides and therefore is deemed too dangerous for our chosen processing route.

2. Experimental procedure

Alloys are prepared by weighing the component elements, such that an approximately 1 cm^3 'button' may be produced by arc melting. The materials are of at least 99.99% purity and in sheet, plate, pellet or powder form prior to fabrication. The melting process is conducted in a Ti-gettered, high purity argon atmosphere. To ensure chemical and microstrucural homogeneity, the buttons are turned and remelted 3–5 times within the furnace. The resultant buttons are then weighed and then (given negligible weight loss) analyzed by optical and scanning electron microscopy (SEM; Philips XL30 FEG with energy-dispersive X-ray spectrometry, EDS). Ribbons of 2–8 mm width, with thicknesses in the region 20–50 μm, are produced from the pre-alloyed buttons by the melt–spinning process. The buttons are reheated above their melting point in an argon or helium atmosphere by induction heating and injected by an overpressure of 500 mbar onto a rotating (1800 rpm) copper wheel (diameter = 50 cm). The buttons may also be cut to appropriate shapes and sizes for arc-casting into water cooled copper moulds, to fabricate cylinders 1 or 2 mm in diameter and 25 mm in length, or 0.5, 0.75 or 1 mm thick plates 5 mm wide and 35 mm in length. The buttons have also been prepared for laser remelting by cutting the buttons to 15 mm diameter hemispheres, followed by grinding and fine polishing to produce a flat surface. Since, during laser treatments, some of the applied energy may be reflected, the surface is fine sand-blasted to improve the absorptiveness, ergo improving the efficiency of the laser processing. The laser remelting process was conducted over a range of processing parameters (which will be specified as appropriate) with a 2 kW Rofin-Sinar Nd-YAG laser, however laser power is always kept at 1750 W, and argon shielding of 10 l/min is always applied. The laser cladding and remelting processes were conducted over a range of processing parameters which will be specified as appropriate with a 2 kW Rofin-Sinar Nd-YAG laser. Spark-erosion cut and de-greased Ti-alloy substrates (10 cm × 10 cm) have been selected for the application of Ti-containing metallic glass-forming alloys. For all samples deposited on the Ti-alloy, the carrying (delivered at 3 l/min) and shielding gas (10 l/min) was argon. Feeding Cu, Zr, Ni, Sn and Si powders from a powder feeder under argon atmosphere, achieved the composition of the layers. The powders were purchased commercially and all were at least 99.99% pure. The Ti-content in the layers was developed solely through dilution from the Ti-substrate. The layers were then remelted at the same parameters as for simple remelting outlined above. All resultant fabrications are investigated by optical microscopy, SEM with EDS (high-resolution) transmission electron microscopy ((HR)TEM) (FEG Jeol 2010) with in situ heating and electron-energy-loss spectroscopy (EELS) capability, and X-ray diffraction (XRD) (Phillips PW1710). Hardness and scratch examinations are conducted on a CSM Revetester with Vickers indenter and Rockwell C type diamond stylus, respectively, while nanoindentation investigations were conducted on MTS Nanoindenter XP with CSM/LFM control. Sliding wear tribo-testing has been conducted on a CSM HT tribometer against hardened (63Rc) 100Cr6 steel disks. Variances in contact stress, wear test speed and counterface roughness were investigated during wear testing. The test speeds were 10 or 20 cm/s and will be noted where appropriate. Confocal optical microscopy (μSurf Nanofocus Messtechnik) was additionally implemented in the characterization of the worn surfaces.

3. Results and discussion

3.1. Effect of processing on microstructure

It is common practice to prepare metallic ribbons by induction melting a glass-forming compositional blend and 'injecting' it onto a large rotating copper wheel. This results in solidification which is often rapid enough to prevent crystal nucleation and growth, i.e. form bulk amorphous material. Fully amorphous metallic ribbons are attainable and this has been confirmed by TEM (with EELS), XRD and also by differential scanning calorimetry (DSC), with no microstructural differences found between processing in argon or helium.

The concepts of amorphous materials may be explored in this way; however their practical use and indeed mechanical testing possibilities are limited. Typical ribbon thicknesses are less than 100 μm (in those prepared for this investigation ∼30 μm) and widths are a few mm. In order to prepare larger samples, and samples for laser remelting, as cast samples of chosen glass-forming alloys are prepared in argon atmosphere by arc-casting. For the $Cu_{47}Ti_{33}Zr_{11}Ni_6Sn_2Si_1$ alloy, generally a microstructure consisting of a fine eutectic matrix, which surrounds Ti-rich dendrites and Zr–Sn based crystals, was found. This will be seen clearly later.

Arc cast plates of various compositions, 35 mm in length, 5 mm in width and 0.5, 0.75 or 1 mm in thickness have been prepared and investigated using TEM. One example is the $Cu_{50}Zr_{30}Ti_{10}$ alloy, which when cast to 0.5 mm plates, and examined by XRD revealed an amorphous halo overlain with several crystalline peaks. When TEM investigation is implemented, a large portion of the sample was found to be amorphous. Other areas revealed homogeneous, however, spa-

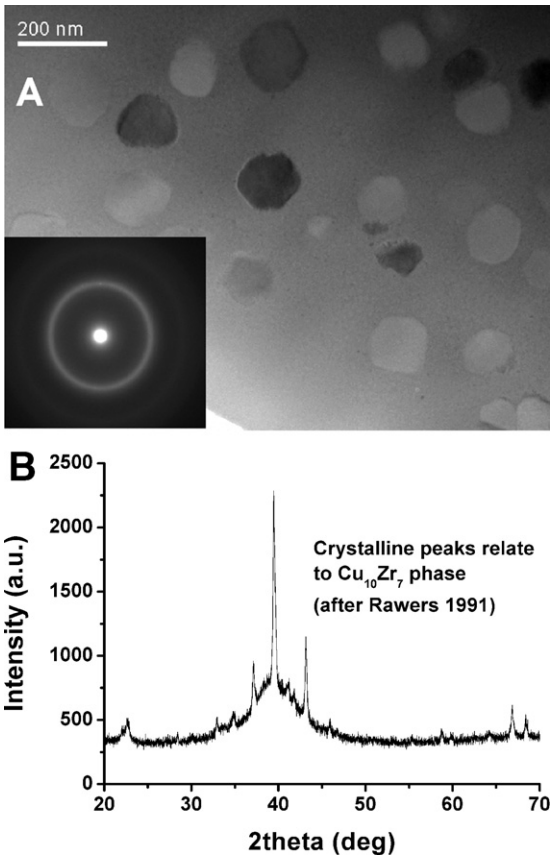

Fig. 1. (A) Ref. [12] reveals the structure found at the base of an arc-cast 0.5 mm plate with the matrix amorphicity confirmed by the inserted diffraction ring in (A); (B) an XRD scan revealing the presence of $Cu_{10}Zr_7$ [13] crystals overlain on an amorphous halo.

tially limited, dispersions of 50–100 nm sized crystals embedded within the amorphous matrix (Fig. 1A (including the accompanying diffraction ring inset from the amorphous matrix)). In situ EDS examination showed these crystals to be of average composition: $Cu_{50}Zr_{38}Ti_{12}$. This relates very well to the crystalline phase found in the XRD examination (Fig. 1B), whose peaks correspond to those of the intermetallic phase $Cu_{10}Zr_7$ as published by Rawers [13]. The difference in microstructure is the result of differing cooling rates within the copper mould. The 'bottom' of the plate (i.e. from the base of the mould, away from the arc heat source) is subjected to rapid and 'instantaneous' cooling, which leads to an amorphous structure. The top of the plate is subject to some 'residual' heating by the leftover melt of the button and, therefore, the plate in this area has enough time to nucleate and grow crystals of the size shown in Fig. 1. For the comparative wear experiments, shown later, $Cu_{47}Ti_{33}Zr_{11}Ni_6Sn_2Si_1$ alloy was used and has been investigated to reveal a fully amorphous structure.

Laser remelted tracks have been fabricated with amorphous properties. The results here will focus on tracks produced by laser remelting of a $Cu_{47}Ti_{33}Zr_{11}Ni_6Sn_2Si_1$ alloy. The results shown are concerned with single tracks (1.2 mm wide) produced at power = 1750 W, table speed = 133 mm/s, beam defocus = −6 mm and overlain tracks with the same parameters with laser head displacements of 1.0 and 1.1 mm. Amorphous layers up to 300 μm in depth can be produced. A heat-affected zone thereafter exists (Fig. 2A and B), which (in this example) consists of Ti-rich dendrites (dark areas) seemingly maintained within a chemically homogeneous amorphous matrix (Fig. 2B and C). This shows that despite the temperature in this area not being sufficient to melt the associated dendrites, the cooling rate is high enough to form an amorphous matrix, which initially shows a fine eutectic form. This is a very important observation in terms of creating an amorphous matrix, which can be reinforced by particle injections. Confirmation of structure and chemistry of the laser melted track, along with the

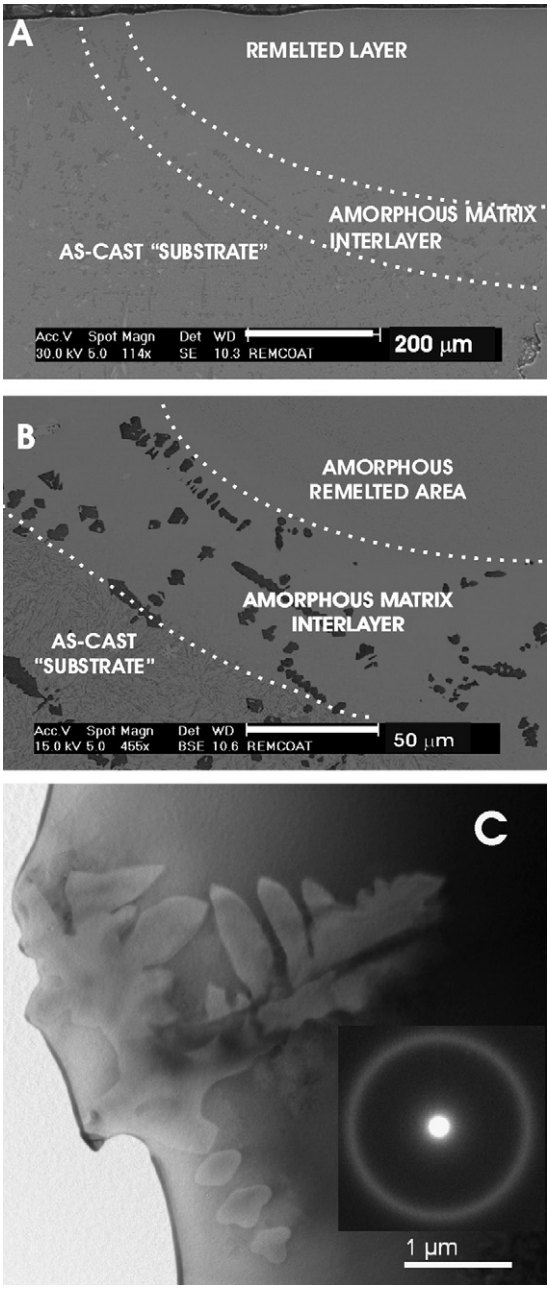

Fig. 2. (A) SEM image highlighting the laser remelted $Cu_{47}Ti_{33}Zr_{11}Ni_6Sn_2Si_1$ alloy track and (B) heat-affected zone exhibiting Ti-rich dendrites in an amorphous matrix and (C) a TEM image revealing a Ti-rich dendrite in the amorphous matrix from the amorphous matrix interlayer.

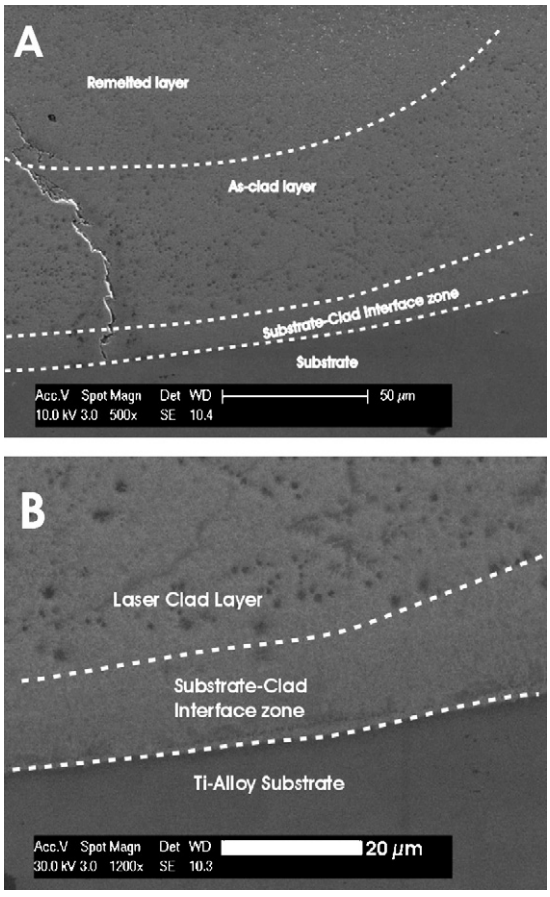

Fig. 3. (A) SEM image revealing the zones of a clad and remelted metallic glass-forming layer on a Ti-alloy substrate, with (B) revealing more detail from the interfacial area.

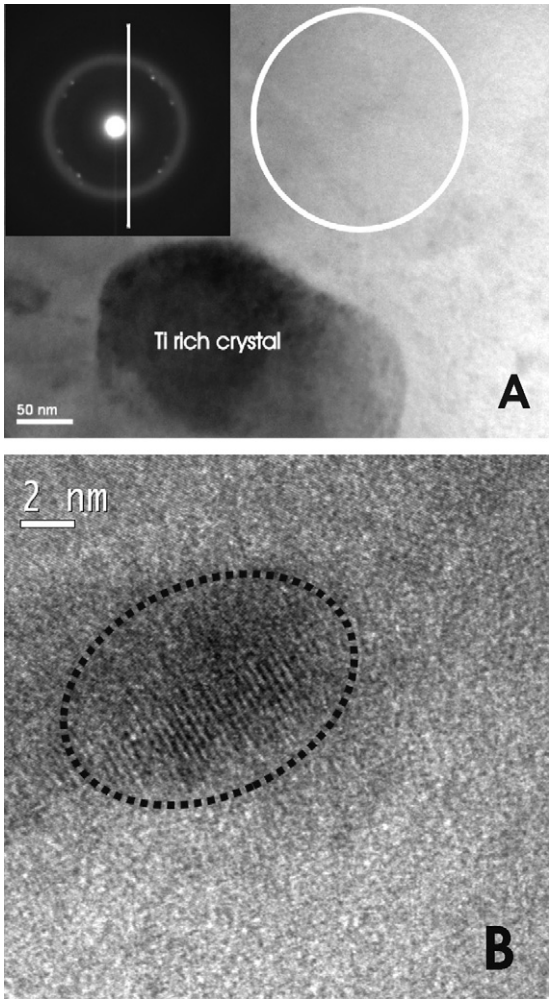

Fig. 4. (A) A 200 nm Ti-rich crystal from a laser clad and remelted layer, retained within an amorphous matrix (confirmed by the diffraction insert taken at the white ring). (B) A HRTEM image of a 5 nm size Ti-rich crystal bound in an amorphous matrix.

retained dendrites was taken by TEM (with EDS) investigations (see Fig. 2C).

In the instance of a clad and remelted layer (Fig. 3A and B), the composition $Cu_{47}Ti_{33}Zr_{11}Ni_6Sn_2Si_1$ was again chosen for investigation. The layer forms featureless regions, indicating that rapid cooling is achieved; the cooling rate is too low, however, to form a fully amorphous layer at the prescribed treatment conditions. The advantage of this is that a thicker layer may be attained, and the mechanical properties between the layer and the substrate may be more evenly graded. Upon remelting, however, the faster cooling also leads to higher stresses being developed within the layer, and these are often released by cracking, which may propagate to the as-clad region (Fig. 3A). Fig. 3B shows that the bonding is good, while the composition was confirmed by EDS, to be that of $Cu_{47}Ti_{33}Zr_{11}Ni_6Sn_2Si_1$, at the track centre, in accordance with that expected. It should be noted that the entire Ti-portion of the layer was derived from the substrate by dilution.

TEM observations from the remelted area (an example is shown in Fig. 4) show that some areas are amorphous in nature. There is a greater proportion of crystalline content than amorphous with the crystals being for the order of 5 nm (signifying nucleated grains during the laser processing) and grains up to 2 μm, which, due to their relatively large size may indicate retained grains that were not melted during laser processing.

3.2. Hardness and scratch observations

The hardness results are summarized in Table 1, together with their *H*/*E* relationship [14,15]. All samples were investigated by micro and/or nanoindentation to reveal information about the

Table 1
Hardness (*H*), elastic modulus (*E*) and *H*/*E* values for $Cu_{47}Ti_{33}Zr_{11}Ni_6Sn_2Si_1$ samples produced according to the various denoted processing routes [12]

Processing route	Hardness, *H* (GPa)	Young's modulus, *E* (GPa)	*H*/*E*
As-cast precursor[a]	650 HV0.2		
Melt–spun ribbon	14.9	171	0.087
Cast plate (1 mm):			
Edge	14.1	174.2	0.081
Middle	13.35	167.9	0.079
[a]	750 ± 20 HV0.2		
Laser remelted track	12.4	153.4	0.081
[a]	785 HV0.2		

[a] Hardness values in Vickers.

hardness attainable by the various processing routes. Given the complex structure and large differences in grain sizes within the crystalline sample, it was decided that nanoindentation was not a suitable test method for this sample. Likewise, given that the thickness of the ribbon was only 20–30 μm, it was deemed unsuitable to subject this sample to micro-hardness testing. The results show that there is a variation between the samples, however not so significant, indicating that the processing route does not radically affect the amorphous nature (at least in terms of medium to long range order) of the samples. It should be noted that a Poisson ratio of 0.35 was assumed for the samples given their amorphicity and ergo lack of ductility. It is therefore possible that the Young's modulus may be lower than recorded, which would lead to a higher *H*/*E* value, stipulated as being significant for good wear resistance [14,15].

The fact that the nanoindentation result for the arc-cast plate is higher at the edge than at the middle can be attributed to the fact the edges were in direct contact with the mould wall, and therefore experience differing (much faster) cooling conditions than for the bulk of the sample. For the time being we shall only consider the middle (bulk) values of the arc cast plates, which is valid since all samples that were wear tested were cut from the centre of the plates. It is interesting to see that while there is a spread of data as regards hardness and Young's modulus across the three samples, the laser remelted track and arc-cast plate share similar *H*/*E* values, while the melt–spun ribbon bears a markedly higher *H*/*E* value. These are, in turn, widely different to the results obtained for the crystalline material, which is in the region of 18% lower than the amorphous layer. This is in accordance with previous studies on the comparative hardness and elastic modulus of crystalline and amorphous materials [16]. Any slight deviation from this expected difference can be accounted for in the fact that the matrix of the crystalline material has a very fine eutectic structure, which is reflected in the ease with which it forms an amorphous matrix as stated previously.

Problems do occur however when overlapping tracks are administered instead of single, or adjacent tracks; particularly in the overlapping region where some recrystallization is allowed to occur. As an example, $Cu_{47}Ti_{33}Zr_{11}Ni_6Sn_2Si_1$ formed a 10–20 μm dendritic interlayer upon overlapping. The hardness values for the amorphous remelted layer and this dendritic interlayer were found to be 785 and 745 HV0.2, respectively, so while the difference is not great, it is an area which may cause problems in an industrial application, for example, in tribological contacts.

Both microscale and nanoscale indentations in all samples were seen to induce the formation of shear bands, which are indicative of amorphicity, since the stress induced by the indentation cannot be dissipated in grain boundaries (for example). This leads to one limitation of metallic glasses in their lack of plasticity [17] often induced through thin, sheet-like volumes in which very large strains can be concentrated, leading to the formation of shear bands. Fig. 5A shows how these bands form in the amorphous regions of the laser remelted $Cu_{47}Ti_{33}Zr_{11}Ni_6Sn_2Si_1$ alloy under indentation (left) and a scratch edge (right). The hardness in the amorphous matrix layer was recorded at around

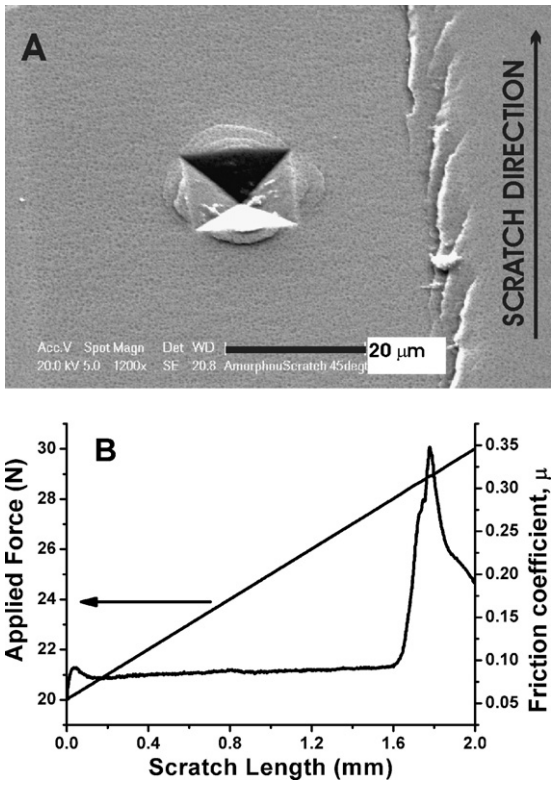

Fig. 5. (A) Vickers indent with shear band formation in an amorphous laser remelted layer, adjacent to shear bands formed during scratch testing. (B) A typical scratch curve revealing material friction coefficient response to the applied load over a 2 mm scratch length.

650 Vickers, with the retained crystals of course playing a role in this value. This indicates that the layer provides a (functional) gradient between the amorphous layer and the substrate.

The samples were also subjected to scratch testing against a Rockwell C diamond stylus. A typical result for an increasing load from 20 to 30 N is shown in Fig. 5B. The results show that the layers are capable of very low friction coefficients ($\mu < 0.1$) for single pass testing so long as severe plastic deformation is not initiated in the scratch contact. The critical value for this behaviour was found to be 28 N for $Cu_{47}Ti_{33}Zr_{11}Ni_6Sn_2Si_1$ alloy fabricated by laser remelting. At this value (as is seen in Fig. 5B), the adhesion component of the friction coefficient suddenly increases with material smearing. In Fig. 5A, a single Vickers hardness indent is seen adjacent to a scratch edge, as stated previously. The formation of shear bands is clear to see in both cases.

When scratch testing is performed on samples exhibiting crystals embedded in an amorphous matrix, the amorphous material is seen to accommodate plastic deformation in shear bands as would be expected, while the crystalline phase (here it is a Ti-rich dendritic phase), responds in several interesting ways. Fig. 6 shows a network of shear bands in the amorphous phase resulting from the scratch test. When the crystals are found to be exposed to the counterface, the crystalline phase is found to be ductile and in some cases adheres to the diamond stylus. This in turn promotes high local stresses and material smearing, as highlighted in Fig. 6A. The shear bands are generally seen to

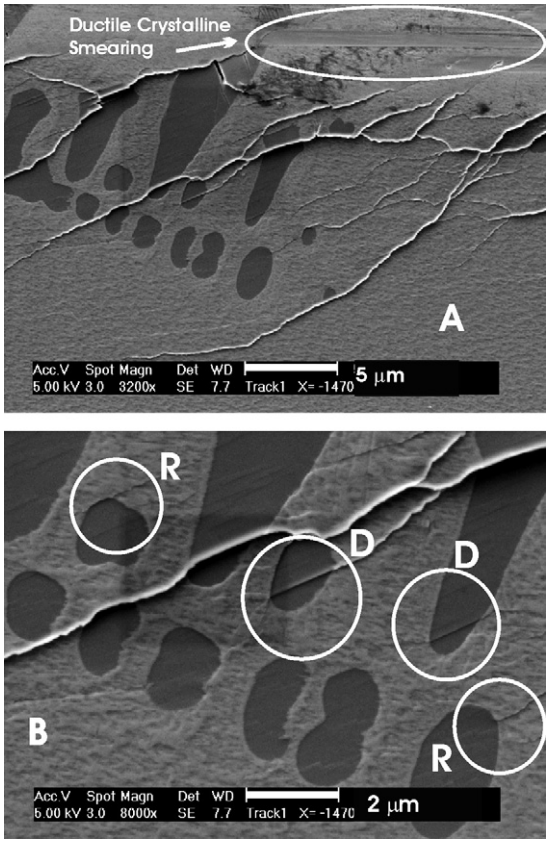

Fig. 6. SEM images revealing the effect of a crystalline phase on shear band propagation: (A) overview of a shear band network and ductile smearing, and (B) detailed view of shear band retardation (*R*) or deflection (*D*) in the crystalline phase.

follow a 'random' path, however they are either retarded (highlighted as *R*s in Fig. 6B) or deflected to follow a shear plane in the crystalline phase (highlighted as *D*s in Fig. 6B).

This observation is important for the design of amorphous layers and indicates that amorphous matrix layers may be more favourable than solely amorphous layers, although the relative size, proportions and distributions of these constituent phases should also be considered [18]. Such a constituent layer was seen in the laser cladding and remelting layers and they too exhibit very high hardness values. The hardness of the as-clad region was found to be slightly lower (670–700 HV0.2) than the remelted area (850–890 HV0.2), as expected (Fig. 7A). This is due to the enhanced cooling afforded by the rapid scan speed and subsequent refinement of the microstructure. It is also interesting to note, in terms of functionally grading, not only a coating, but also the coating–substrate system, that the hardness of titanium substrate was significantly increased after treatment to a depth of over 200 μm beyond the clad layer. The hardness in this area was 425 HV0.2, while the hardness of the substrate 1 mm away from the clad layer was only 300 HV0.2. The increased 'remelt depth' and heat effects on the titanium substrate are a direct consequence of the poor thermal conductivity of titanium. Again, the indentation method appears to induce shear band formation (Fig. 7B), which indicates that the layer may have amorphous constituent regions. This is very promising, since this procedure involves the deposition of a five element powder mix. The scratch test results for this coating were also highly promising as the results showed the layers to exhibit a friction coefficient of only 0.035 at 20 N loads and 2 mm/min scratch speed. This is even less than the pure amorphous layers and no shear banding was induced. This result may of course be a result of the slightly higher hardness of the laser clad and remelted layers, which leads to a shallower indent, which in turn reduced the ploughing component of friction coefficient.

3.3. Wear observations and the effect of counterface roughness

Given the observations surrounding the different processing routes and their effect on the material characterization, it was predicted that there may be differing responses to wear given developments in specific criteria for good wear resistance of glassy metal systems [15]. A second prediction was also considered by differing the roughness of the counterface. By considering the equation for determining the so-called plasticity index (Eq. (1)) [19], which assumes surface geometry and topography to be the determining factors in the amount of plastic deformation (thereby neglecting load), it may be possible to predict the effect of counterface roughness on the deformation process of tribological contacts. The expression for the plasticity

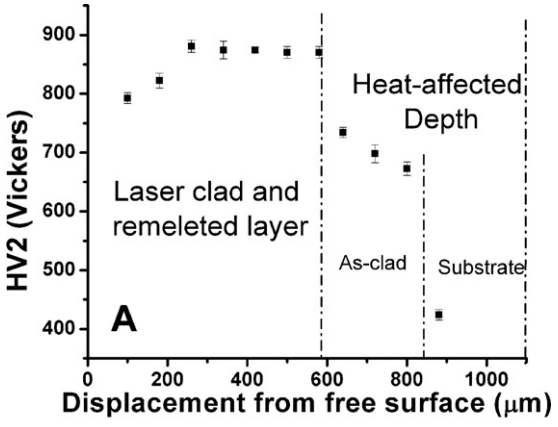

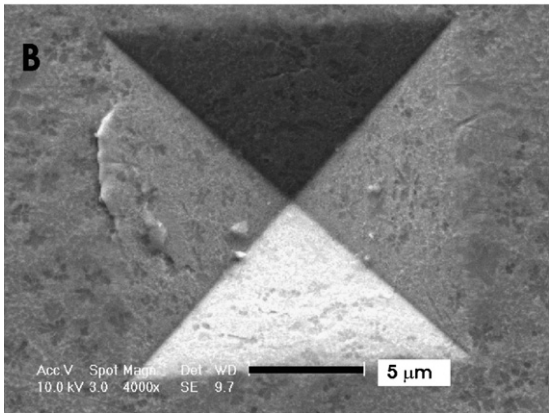

Fig. 7. (A) Hardness profile of a laser clad and remelted layer of $Cu_{47}Ti_{33}Zr_{11}Ni_6Sn_2Si_1$ composition and (B) Vickers indent from the centre of that layer revealing shear banding.

index (ψ) is shown here:

$$\psi = \frac{E'}{H}\sqrt{\frac{\sigma}{\beta}} \quad (1)$$

where E' is defined as:

$$E' = \frac{1}{(1-\nu_1^2)/E_1 + (1-\nu_2^2)/E_2} \quad (2)$$

In Eq. (2) ν is the Poisson ratio and E is the elastic modulus of the contact surfaces (denoted by the subscripts 1 and 2). In Eq. (1), σ represents the standard deviation of the asperity height distribution and β is the radius of the asperity tips. Bearing this in mind, it is clear to see that an increase in the σ will lead to an increase in ψ. Given that the following bounds hold true for Eq. (1),

$\psi > 1$ ➔ significant plastic flow
$0.6 < \psi < 1$ ➔ mixed elastic/plastic conditions
$\psi < 0.6$ ➔ plastic flow unlikely

then it is clear that the asperity distribution of an unpolished surface leads to an increased probability of plastic deformation compared to the polished surface. One may therefore predict an unpolished counterface, or rougher surface, to lead to higher amounts of plastic deformation, which, in the instance of glassy metals, is exhibited in the formation of shear bands.

All samples were subjected to several different load and speed conditions in the wear testing and some results are summarized in Table 2, with the wear rate calculated according to the well-known Archard wear equation for sliding contacts, with the wear volume proportional to the normal load and sliding distance. Wear and friction curves for the crystalline, 1 mm thick plate and laser remelted coatings are seen in Fig. 8 for tests conducted under dry sliding wear conditions.

It is clear that the amorphous material in plate form has a characteristically lower friction coefficient (0.5) than the crystalline material (0.7), while the amorphous layer produced by high power laser has a friction coefficient in the mid-range of these two (0.6), with the baseline being comparable to that of the amorphous plate, and the upper fluctuation level being slightly lower than that of the crystalline material. This is easily explained due to the microstructural mismatch caused due to the overlapping areas, which induce narrow recrystallization bands between a

Table 2
Example test parameters and results of wear tests (all test speeds = 10 cm/s)

Sample type and processing	Contact stress (MPa)	Friction coefficient	Wear rate ($\times 10^{-6}$ mm^3/N m)
100Cr6 ball	4.3	0.55	1.64
Crystalline	3.5	0.75	2.54
Ribbon	2.1	0.5 → 0.7	2.39
1 mm arc cast plate	5	0.5	2.02
Single laser track:			
Initial wear stage	4.8	0.5 → 0.7	2.13
Final wear stage	4.8	0.7 → 0.9	1.43
Laser remelted coating	3.2	0.5 → 0.7	3.08

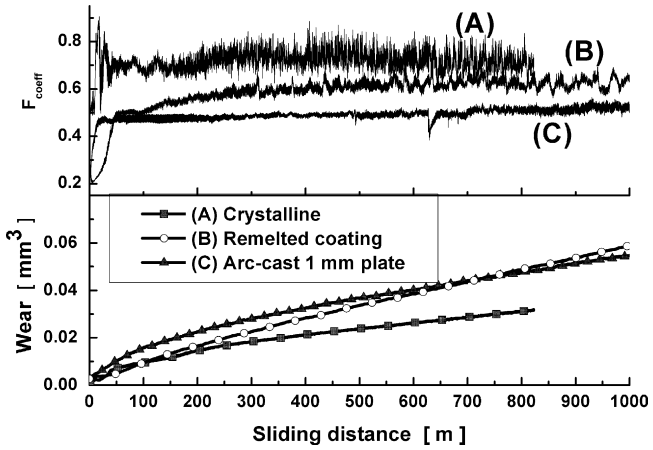

Fig. 8. Wear and friction curves for: (A) crystalline (B) arc-cast plate and (C) laser remelted $Cu_{47}Ti_{33}Zr_{11}Ni_6Sn_2Si_1$ alloy.

pre-remelted layer and the new, overlapping layer. Some samples exhibited a steady increase in friction (identified in Table 2 by the '→' symbol). This was found to correlate with those samples whose amorphous/crystalline ratio decreased during the wear test, with higher friction resulting from crystalline/crystalline contacts than for amorphous/crystalline contacts. The single track laser remelted tracks were found to have higher fluctuations in friction coefficient and this may is explained schematically in Fig. 9. As the single track sample wears away, the percentage crystalline contact increases, while the amorphous overlap coating may be cut to the same size, and yet only has crystalline contact areas in the track-overlap areas. The wear values for the three samples are similar, however the crystalline sample was tested against a polished disk ($R_a \sim 8$ nm), and the other two examples shown were tested against unpolished disks ($R_a \sim 0.3$ μm).

The crystalline material has good wear properties and this is not surprising since it consists of a very fine eutectic matrix and well bound needles and dendrites, which do not break free from the matrix easily. The results attained for the amorphous samples are similar to work by Fu et al. [20] in that exceptional wear properties for amorphous materials have not been conclusively proved for dry sliding wear conditions; however, under rolling contact conditions, the wear resistance of Zr-based BMG has been found to be almost twice as high as for steel rollers [21].

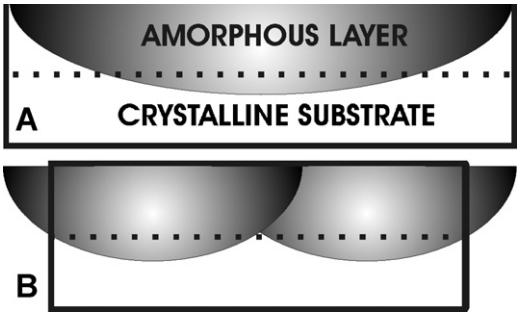

Fig. 9. Schematic representations of: (A) a single track wear contact and (B) overlapping wear tracks the dash line represents a possible level of material removal reached after some wear period.

The wear properties of the layers are also encouraging, with wear performance seen to be comparable to the 100Cr6 steel in agreement with Refs. [22,23] and of the same order as some MMC layers tested under boundary lubrication conditions [4]. For the fully amorphous materials (ribbons and plates), an increase in speed was seen to lead to a decrease in wear rate, which can be attributed to the faster formation of shear bands, and possible higher density thereof, thus distributing the local high contact stress areas more evenly over the wear surface. Fig. 10A reveals the vein-like structure synonymous with such shear band formation on the worn surface of the 1 mm arc-cast plate. The 'inverse' picture (Fig. 10B) provides proof that the features are not cracks, but indeed shear bands, indicated by the height fluctuation (light areas on the left appear shadowed on the right when the sample is inverted with respect to the electron detector). It is notewor-

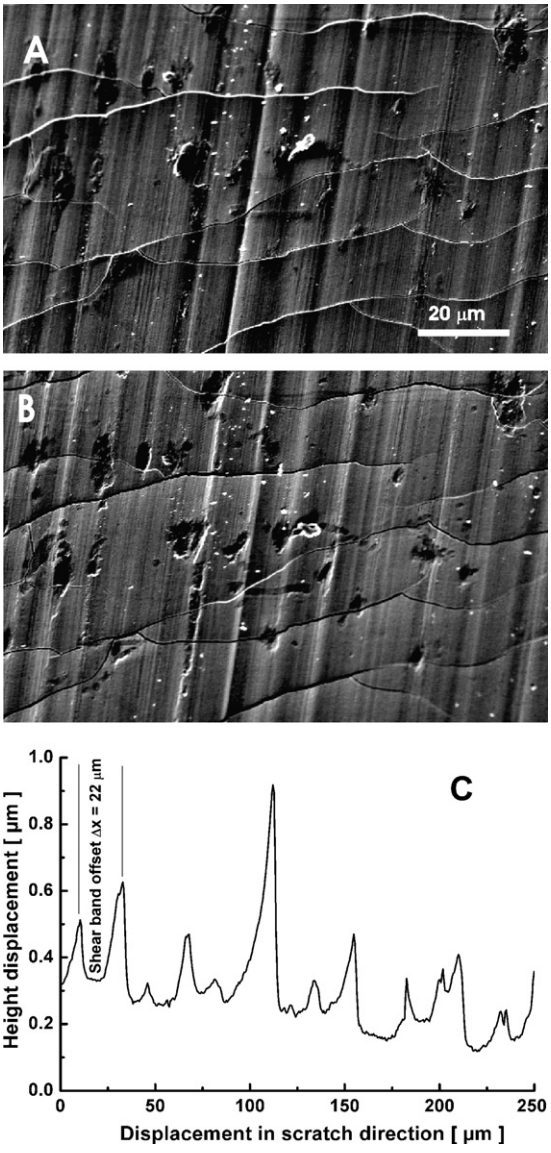

Fig. 10. (A) SEM image of shear bands formation in $Cu_{47}Ti_{33}Zr_{11}Ni_6Sn_2Si_1$ alloy 1 mm plate due to sliding wear, (B) sample rotated 180° (wear test speed = 10 cm/s; contact stress = 3.6 MPa) [12] and an arbitrary height profile recorded by confocal microscopy is shown in (C).

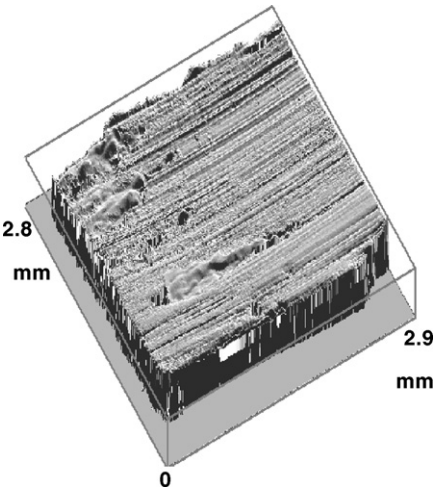

Fig. 11. Confocal micrograph in photorealistic mode showing the appearance of a $Cu_{47}Ti_{33}Zr_{11}Ni_6Sn_2Si_1$ alloy ribbon after a wear test against a polished disc—note no shear bands are formed.

thy that these shear bands form at (more-or-less) 90° to the wear direction, and have an inter-shear band spacing of around 20 μm, as seen in Fig. 10C.

The earlier prediction that the counterface roughness may play an important role in the deformation of amorphous materials under tribological contact has been shown to hold true for rough (R_a = 300 nm) surfaces. For polished (R_a = 8 nm) counterface surfaces, no shear band formation was seen. Fig. 11 shows a confocal photorealistic micrograph for an amorphous ribbon subjected to a contact stress of 2.1 MPa at a test speed of 20 cm/s against a polished disc. The surface appearance is one of 'conventional' hill and groove type wear and no shear banding is seen. Similar results were found for all amorphous samples tested against finely polished counterfaces.

Where shear band formation was found, the height of the shear band steps was found by confocal microscopy to be 0.3–0.6 μm (Fig. 10C). The fact that these shear bands form confirms the very high local stresses present, since the yield point of bulk metallic glasses is of the order of 1000 MPa, yet the calculated contact stress over the worn surface was only around 3 MPa.

Fig. 12A highlights an interesting finding in the wear behaviour of $Cu_{47}Ti_{33}Zr_{11}Ni_6Sn_2Si_1$ alloy 1 mm plate, as it reveals debris build-up behind the shear bands (with respect to the wear direction). This can be seen schematically in Fig. 12B. The debris has two characteristic sizes: ~20 μm size flake shaped particles and ~750 nm size rounded powders. When the shear band asperities begin to break down, the nanoscale debris collected and compacted by oxidative adhesion behind the shear bands, comes back into contact with the counter-disk and break down again takes place. Elemental mapping revealed oxide islands were formed during the wear tests by high local stresses leading to elevated temperatures, which promote oxidation. The debris also revealed high levels of oxidation, which indicates that the material removal mechanism is driven by oxidative wear, in accordance with Ref. [22]. No iron transfer from the counter-body was found by chemical analyses.

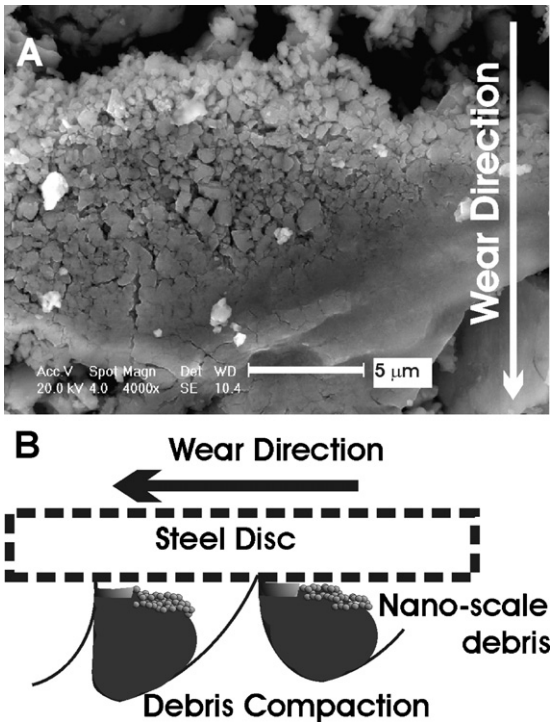

Fig. 12. (A) SEM image revealing appearance of debris pile up behind the shear bands formed perpendicular to the wear direction. This phenomena is revealed schematically in (B) (wear test speed = 10 cm/s; contact stress = 5 MPa).

The laser remelted layer tested at a contact stress of 3.2 MPa and 10 cm/s sliding speed revealed a rather interesting feature in that the shear band formation was not seen perpendicular to the sliding direction as for the plate, but instead, perpendicular to the laser treatment direction. The inter-shear band spacing was again in the order of 20 μm, with the height again being of the order of 0.3–0.6 μm. This was revealed by both SEM (Fig. 13) and confocal microscopy.

These shear bands also appear to be only present within the 'bulk' of the laser track and the directionality of them is very important for several reasons. The first implication is that the shear band formation occurs due to internal stresses within the laser remelted track, which must be greater than the applied stress field, since the treated layer is positioned at 45° to the applied load, and this is coincidental with the position of maximum shear stress. Secondly, this may pose a limitation for the coating if, in practical application, the orientation of a laser treated sample, with respect to its working direction, is so important. A benefit of this however, is that the wear debris cannot accumulate behind the shear bands, but can instead be removed continuously. Given that the size of the final wear debris is very small (sub-micron), it was not seen to change the wear mechanism by becoming third bodies in the wear contact, which is a limitation of crystalline coatings when they begin to break down. An area attributed as being related to the overlapping region of ~150 μm is found to be shear band free, which indicates (as expected) that the overlapping regions are not (fully) amorphous. Furthermore, confocal microscopy for this area revealed the shear band-containing area to be higher than the shear band-free area. The implication here is that the area pertaining to the shear band formation is harder (or at least more wear resistant) than the neighbouring, overlapping area. This is in accordance with the indentation findings.

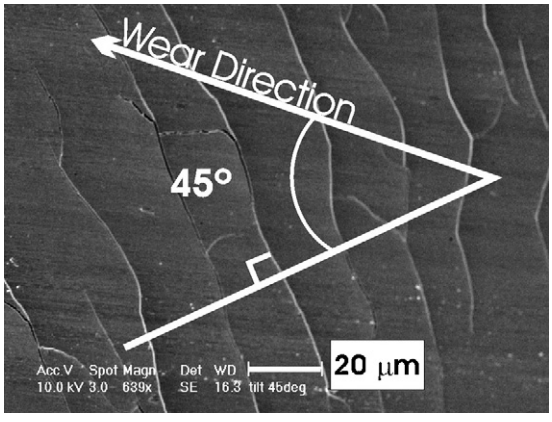

Fig. 13. SEM image revealing shear band formation at 45° to the wear direction, but perpendicular to the laser processing direction.

4. Conclusions

Metallic glasses have been successfully synthesised by a range of processing routes with the production of amorphous layers by high power lasers being proven viable. The thickness of the layers provides excellent opportunities to fabricate layers on material such as titanium which may be functionally graded, since laser cladding readily facilitates well adhered layers up to 1 mm in thickness, and the cooling conditions may be tailored simply by processing speed variations. This layer may then be remelted as shown in this investigation to provide 300 μm layers bonded to the 'precursor layer' by an amorphous matrix interlayer. This reduces the 'egg-shell' effect often found when depositing high hardness layers directly onto soft substrates, and opens possibilities for commercial applications. The hardness of the layers has been found to be very high (>700 HV) and the indentation procedure has been seen to induce shear band formation. The addition of crystals is seen to act as deflectors/retarding obstacles to the shear band propagation. This has been seen to be particularly prevalent in the case of scratch testing. Scratch testing has also shown that the friction coefficients of amorphous metallic alloys may be as low as 0.05 for single pass scratch tests at 20 N. The wear properties of the layers are also encouraging, with wear performance seen to be comparable to the 100Cr6 steel, and of the same order as some MMC layers tested under boundary lubrication conditions. The performance is however, still somewhat limited by shear band formation and internal stresses, and therefore the expectations of excellent wear resistance have not been proven under dry sliding wear conditions. It is interesting to find that the scale of the debris formed during wear testing of amorphous metals is sub-micrometer in size. The debris has been found to compact behind shear bands if the shear bands form perpendicular to the wear direction, but is removed if the shear bands form at an angle to the wear direction. The actual laser cladding of BMG compositions has also proven to be successful, both in terms of coating adhesion, chem-

ical homogeneity, amorphisation, high hardness and low friction coefficients.

Acknowledgements

The authors acknowledge financial support from the Netherlands Institute for Metals Research (NIMR) and the Foundation for Fundamental Research on Matter (FOM-Utrecht). We also acknowledge the contribution of Dr. P.M. Bronsveld for his kind assistance in sample preparation. Prof. H. Davies and Dr. I. Todd at the University of Sheffield, UK, are also gratefully acknowledged.

References

[1] X.H. Lin, W.L. Johnson, J. Appl. Phys. 48 (1995) 6514–6519.
[2] E.S. Park, H.K. Lim, W.T. Kim, D.H. Kim, J. Non-Cryst. Solids 298 (2002) 15–22.
[3] W. Steen, Laser Materials Processing, third ed., Springer, Berlin, 2003.
[4] V. Ocelík, D. Matthews, J.Th.M. De Hosson, Surf. Coat. Technol. 197 (2005) 303–315.
[5] J. Vreeling, V. Ocelík, J.Th.M. De Hosson, Acta Mater. 50 (2002) 4913–4924.
[6] Y.T. Pei, V. Ocelík, J.Th.M. De Hosson, Acta Mater. 50 (2002) 2035–2051.
[7] F. Aubert, R. Colaco, R. Vilar, H. Sirkin, Scr. Mater. 48 (2003) 281–286.
[8] H. Akamatsu, M. Yatsuzuka, Proc. Front. Surf. Eng. (2003) 19–222.
[9] Y.T. Pei, V. Ocelík, J.Th.M. De Hosson, Mater. Eng. A 342 (2003) 192–200.
[10] W. Johnson, MRS Bull. (1999) 42–56.
[11] L. Tanner, R. Ray, Acta Metall. 27 (1979) 1727–1747.
[12] D.T.A. Matthews, V. Ocelík, J.Th.M. de Hosson, in: Bulk Metallic Glasses, P.K. Liaw, R.A. Buchanan (Eds.) TMS, 2006, ISBN 978-0-87339-612-7, pp. 99–108.
[13] J. Rawers, Private Communication 1991, JCPDS-ICDD, PDF Number 421187 (1997).
[14] A. Leyland, A. Matthews, Wear 246 (2000) 1–11.
[15] A. Leyland, A. Matthews, Surf. Coat. Technol. 177–178 (2004) 317–324.
[16] M.J.W. Greuter, L. Niesen, A. van Veen, R.A. Halvoort, M.G.M. Verwerft, J.Th.M. De Hosson, A.J.M. Berntsen, W.G. Sloof, J. Appl. Phys. 77 (1996) 3467–3478.
[17] J. Schoers, W. Johnson, Phys. Rev. Lett. (2004) 255506.
[18] Y. Pei, D. Galvan, J.Th.M. De Hosson, Acta Mater. 53 (2005) 405–4021.
[19] J.A. Greenwood, J.B.P. Williamson, Proc. R. Soc. London A295 (1966) 300.
[20] X.-Y. Fu, T. Kasai, M.L. Falk, D.A. Rigney, Wear 250 (2001) 409–419.
[21] M.Z. Ma, R.P. Liu, Y. Xiao, D.C. Lou, L. Liu, Q. Wang, W.K. Wang, Mater. Sci. Eng. A 386 (2004) 326–330.
[22] A.L. Greer, K.L. Rutherford, I.M. Hutchings, Int. Mater. Rev. 47 (2) (2002) 87–112.
[23] T. Gloriant, J. Non-Cryst. Solids 316 (2003) 96–103.